J Mater Sci (2007) 42:2724–2734
DOI 10.1007/s10853-006-1275-1

Kinetics, mechanism and modelling of microstructural evolution during thermomechanical processing of a 15Cr–15Ni–2.2Mo–Ti modified austenitic stainless steel

Sumantra Mandal · P. V. Sivaprasad · R. K. Dube

Received: 19 July 2005 / Accepted: 25 January 2006 / Published online: 9 January 2007

Abstract The paper discusses the kinetics, mechanism and modelling of the microstructural evolution of a 15Cr–15Ni–2.2Mo–0.3Ti modified austenitic stainless steel (alloy D9) during dynamic recrystallization (DRX). The experimental methodology included different hot working operations employing industrial equipment such as forge hammer, hydraulic press and rolling carried out in the temperature range 1,173–1,473 K to various strain levels. The kinetics of DRX has been investigated employing modified Johnson–Mehl–Avrami–Kolmogorov (JMAK) model. It has been found that the value of Avrami exponent varies in a close range of 1.17–1.34 which implies that D9 exhibits growth controlled DRX. Optical metallography has revealed that nucleation of DRX grains occurred along the prior grain boundaries by bulging mechanism. Microstructural characterization has shown that a significant correlation between microstructural features and processing parameters exists. However, this interrelation is ambiguous and fuzzy in nature. Therefore an artificial neural network model has been developed to predict the microstructural features, namely fraction of DRX and grain size, at different processing conditions. A good correlation between experimental findings and predicted results has been obtained. An instantaneous microstructure, therefore, can be designed in order to optimize the process parameters based on microstructural evolution.

S. Mandal · P. V. Sivaprasad (✉)
Materials Technology Division, Indira Gandhi Centre for Atomic Research, Kalpakkam, Tamilnadu 603102, India
e-mail: prasad@igcar.ernet.in

R. K. Dube
Department of Materials and Metallurgical Engineering, IIT Kanpur, Kanpur, UP 208016, India

Introduction

Austenitic stainless steels have been chosen worldwide as materials for in-core applications in fast reactors owing to their excellent elevated temperature mechanical properties, compatibility with liquid sodium and adequate resistance to void swelling [1]. Primarily AISI type 316 and its modifications have been used as materials for fuel subassemblies seeing a dose of ≈65 dpa (displacements per atom). However, the severe and hostile operating conditions of commercial fast breeder reactors would demand development of new austenitic stainless steels with improved swelling resistance at damage levels greater than 125 dpa. In order to meet the requirements for the core components of 500 MW(e) fast breeder reactor project (PFBR) in India, a 15Cr–15Ni–2.2Mo–0.3Ti austenitic stainless steel has been developed indigenously [2]. This conforms to ASTM A771 UNS 38660 and is commonly referred to as alloy D9. This is a candidate material for in-core applications as fuel cladding tube and hexagonal subassembly wrapper.

The alloy D9 has to be processed through various hot forming techniques like rolling, forging and extrusion before it is fabricated into final components. During this processing, material undergoes shape change as well as change in microstructure that depends on the process history. Therefore, it is of

paramount importance to understand the kinetics and mechanism of microstructural evolution which, in turn, would help to achieve the required microstructure in the end product.

Alloy D9 undergoes dynamic recrystallization (DRX) during hot working, as it is a low to medium stacking fault energy material [3, 4]. The domain of DRX in this alloy has been identified by generating processing map [5] and is found at temperatures higher than 1,223 K and strain rates in the range 0.01–100 s^{-1}. However, the kinetics and mechanism of DRX behaviour of this alloy is less studied and needs a detailed physical understanding and experimental evidences. Therefore, in the present study, kinetics and micromechanism of the dynamic processes of this alloy has been investigated by performing various industrial scale metal forming processes such as hammer forging, hydraulic press forging and rolling. These hot forming operations have been carried out in a wide range of temperatures and strains in order to understand the complete DRX behaviour.

Finally, an attempt has been made to establish a model for microstructural evolution of alloy D9 during hot forming. However, it is well known fact that microstructural evolution in hot forming has fuzzy characteristics [6]. Therefore, it is too difficult to use a single mathematical model to represent microstructural evolution during thermomechanical processing of alloy D9. Artificial neural network (ANN), on the other hand, has the inherent capability to deal with fuzzy information, whose functional relation is not clear. Therefore, in the present study, an ANN has been employed to model the microstructural evolution of alloy D9 during hot forming.

Materials and experimental

Materials

The alloy D9 used in the present investigation was supplied by M/s. MIDHANI, Hyderabad, India, in mill-annealed condition as 30 mm diameter rods. Chemical composition of the alloy is given in Table 1. The cast ingots were hot forged and hot rolled to 30 mm diameter rounds. Cold swaging operation was performed in order to reduce the diameter of the rod to 20 mm. The cold swaged rod was then annealed in a vacuum furnace at 1,323 K for 1 h in order to eliminate the work hardening effect of cold working operations as well as to get complete recrystallized structure. From this solution annealed rod, 30 mm height and 20 mm diameter compression specimens for forging operation were machined. For rolling, 24 mm thick rectangular plates were machined from the initial 30 mm hot rolled and hot forged rounds.

Hammer forging and hydraulic press forging

Hammer forging operations were carried out with a 250-kg pneumatic hammer in a single blow in the temperature range 1,223–1,423 K in steps of 50 K. Temperature during the operation was monitored based on the data obtained from cooling curve, which has been established for the present study. The mean strain rate of the forge hammer has been measured by high-speed photography and was found to be 100 s^{-1}. True strains of 0.1, 0.2, 0.3, 0.4 and 0.5 were imparted at each temperature in order to study the effect of strain. The specified amount of strain in each sample was achieved in a single step. As soon as the operation was completed, the deformed specimen was water quenched within 2–3 s in order to freeze the deformed microstructure.

Hydraulic press-forging tests were performed on a 250-ton triple-action hydraulic press. The operations were carried out in the temperature range 1,223–1,373 K in steps of 50 K and similar amount of strains were given at each temperature as mentioned in forge hammer operation. The calculated mean strain rate was equal to $\approx$0.22 s^{-1}.

Rolling

The rolling operations were performed in a 2Hi/4Hi-instrumented laboratory rolling mill (Carl Wezel Model No. 420/350/275). The mill was fitted with a 2Hi hot-roller set, the roller being 420 mm in width and 350 mm in diameter. Tests were carried out in the temperature range 1,173–1,473 K (in steps of 100 K) at a roll speed of 16 rpm, and a true strain of 0.3 was achieved in a single step. The mean true strain rate during rolling was estimated using the following equation:

Table 1 Chemical composition (in wt.%) of 15Cr–15Ni–2.2Mo–Ti modified austenitic stainless steel (alloy D9)

C	Mn	Si	S	P	Cr	Ni	Mo	Ti	B	Co	N
0.052	1.509	0.505	0.002	0.011	15.051	15.068	2.248	0.31	0.001	0.01	0.006

$$\dot{\varepsilon} = v\frac{\ln\left(\frac{h_0}{h}\right)}{\sqrt{R\Delta h}} \quad (1)$$

where v is the peripheral speed of the work roll = 16 rpm, R is the undeformed roll radius = 175 mm, h_0 is the thickness of the plate before rolling = 24 mm, h is the thickness of the plate after rolling = 18 mm and Δh is = $(h_0 - h)$. The calculated mean strain rate was found to be $\approx 2.6\ s^{-1}$.

Characterization

The hot worked samples were cut along the longitudinal direction and one half of the sample was taken to prepare metallographic specimens. Metallographic specimens were polished and etched in 10% ammonium persulphate [$(NH_4)_2S_2O_8$] solution. The microstructures were examined optically in the maximum deformation zone of the samples and grain sizes were measured employing linear intercept method.

Hardness measurements were carried out by Microhardness tester [HMV-2000 SHIMADZU] using 200-g load. The measurements were taken on the maximum deformation zone of the sample. Fraction of recrystallization (%DRX) at different working conditions was calculated employing the following equation:

$$\%\mathrm{DRX} = \frac{H_{\mathrm{CW}(x)} - H_{\mathrm{HW}(x)}}{H_{\mathrm{CW}(x)} - H_{\mathrm{SA}}} \quad (2)$$

where $H_{\mathrm{CW(x)}}$ denotes the hardness of the cold worked specimen at a strain level of x percent, $H_{\mathrm{HW(x)}}$ is the hardness of the hot worked sample at same strain in a particular working temperature at which we want to find out the fraction of recrystallization, and H_{SA} denotes the hardness of solution annealed sample. To obtain $H_{\mathrm{CW(x)}}$, cold working operation of alloy D9 at various strain levels were carried out by high strain rate compression testing machine at room temperature. Similar approach, as depicted in Eq. 2, have been adopted by Sakai et al. [7] to evaluate the degree of softening in polycrystalline nickel after hot working employing flow stress value. Liu et al. [8] have also employed similar hardness method to calculate the fraction of recrystallization in Al alloy.

Results and discussion

Kinetics of DRX

The Johnson–Mehl–Avrami–Kolmogorov (JMAK) model has been widely used to describe the kinetics of recrystallization process [9]. According to this model, recrystallization behaviour at a given temperature should follow the relationship:

$$X_v = 1 - \exp(-kt^n) \quad (3)$$

In this equation X_v is the recrystallization fraction at any annealing time t, k is a constant and n is the Avrami exponent or JMAK exponent. Experimental recrystallization kinetics measurements are usually compared with the JMAK model by plotting $\ln(-\ln(1 - X_v))$ against $\ln(t)$. According to Eq. 3, this should yield a straight line of slope equal to the exponent n.

However, this JMAK model suits better for static recrystallization where annealing time t is available. For dynamic recrystallization, this model in present form could not be applied to investigate the kinetics. This is because in case of DRX, the whole operation finishes in a fraction of second. So time t could not be measured with present experimental facilities.

In the present study, some modification of JMAK model has been carried out in order to investigate the kinetics of DRX. The t term was replaced by ε, where ε is true strain. The modified JMAK model can be expressed as follows:

$$X_v = 1 - \exp(-k\varepsilon^n) \quad (4)$$

Here X_v is the fraction of DRX which has been calculated employing Eq. 2. According to this modified model, if X_v versus ε is plotted, it should yield a sigmoidal curve. In Fig. 1a, the plot of X_v versus ε for forge hammer operation has been drawn. From this figure one can see that the curves are sigmoidal in nature. At high temperatures, the curves are steeper compare to those at low temperatures. This is because at high temperatures, available thermal activation energy is more, which helps the process to be completed in shorter times. Though the trend of these sigmoidal curves is almost consistent, a deviation can be observed at 10% deformation level in 1,273 K which is showing higher extent of DRX. The most possible reason of this variation could be post dynamic softening that may have taken place due to slight delay in quenching. Post dynamic softening like metadynamic recrystallization (MDRX) can readily takes place with little delay in quenching and thereby increases the volume fraction of recrystallization.

Another important observation is made in Fig. 1a is that the recrystallization process is not completed in 1,423 K during hammer forging though it is completed at 1,373 K. This behaviour can well be explained on the basis of a simple model of DRX in terms of rate of

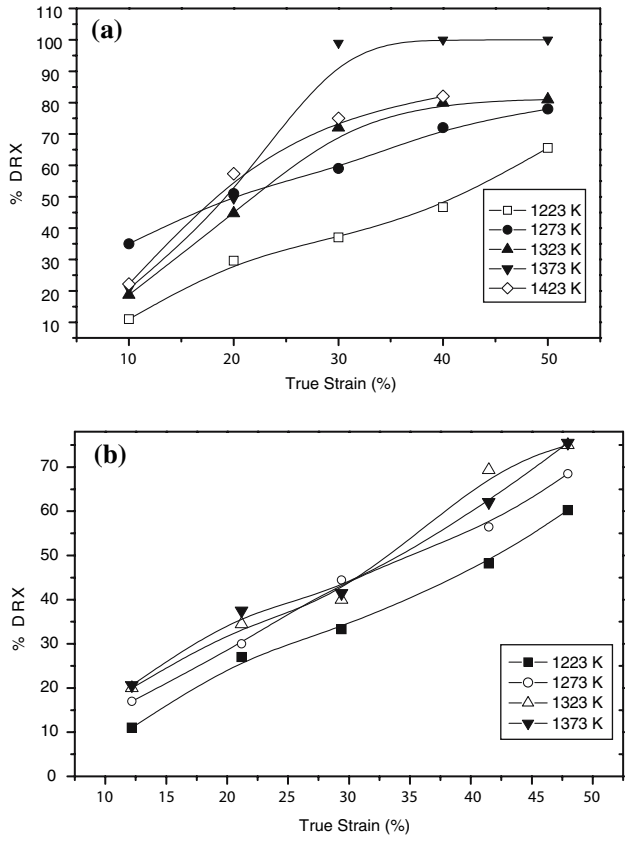

Fig. 1 Effect of true strain on recrystallization kinetics at various temperatures during (**a**) forge hammer and (**b**) hydraulic press operation

nucleation versus rate of grain boundary migration. Alloy D9 is a low to medium staking fault energy (SFE) material. Therefore rate of nucleation will dominate over grain boundary migration [10]. The rate of nucleation can be expressed as

$$\dot{N} = \left(\frac{\beta\dot{\varepsilon}}{bl}\right) \exp\left[\frac{-Q}{RT}\right] \tag{5}$$

where β = constant, $\dot{\varepsilon}$ = strain rate, b = Burgers vector, l = dislocation segment length, Q = activation energy for diffusion, R = gas constant and T = temperature. Since alloy D9 is basically a Ti modified stainless steel, TiC precipitates are likely to take place in the matrix during straining. These precipitates will pin the dislocations and thereby reduces the link length 'l' (Eq. 5) which eventually favours DRX. TiC precipitates, in fact, were found to facilitate DRX in alloy D9 with Ti/C ratio of 8 where the extent of DRX was found much higher as compared to alloy D9 with zero Ti at identical processing conditions [11]. However, if the processing temperature becomes too high, dissolution of these precipitates would happen; thereby the favourable conditions of DRX offered by precipitates will be substantially lost. In yet another study by the authors on the effect of annealing temperatures in the range 1,323–1,573 K on engineering properties for alloy D9, it was found that the amount of precipitates decreases with increasing annealing temperature [12]. From the present study, it seems 1,373 K is the optimum processing temperature for alloy D9 where the complicated interactions between precipitates and processing parameters (i.e. strain, strain rate and temperature) are just sufficient to complete the DRX process. On the other hand, 1,423 K is a higher range of temperature where dissolution of the TiC precipitates may take place; thereby the rate of nucleation will be lowered despite the fact that available thermal activation energy is more as compared to 1,373 K. The detailed investigations using electron microscopy of these samples forms the basis of further course of study.

The modified Avrami plot has also been drawn for hydraulic press forging and is shown in Fig. 1b. These curves are also sigmoidal in nature. However, the curves for higher temperatures, i.e. 1,323 and 1,373 K are not steep, as found in the case of forge hammer operation. The reason could be attributed to the lower strain rate of hydraulic press. As the strain rate for hydraulic press is low, there is always some temperature drop and hence the process could not be completed even at maximum temperatures and strains.

According to the modified JMAK model, if $\ln(-\ln(1 - X_v))$ versus $\ln(\varepsilon)$ is plotted, it should yield parallel straight lines whose slope would be equal to Avrami exponent n. Such relationship is plotted and is shown in Fig. 2a, b. From these figures one can see that the plots are straight line in nature. The straight lines are almost parallel for both the forge hammer and hydraulic press operations. Therefore, it can be corroborated that modification carried out in JMAK model is well supported by the experimental results.

The values of Avrami exponent (n) at different hot-working operations are summarized in Table 2. As can be seen from the table, the value of n varies in the close range 1.17–1.34. The variation of the Avrami exponent is associated with the transition from cyclic to single peak DRX [13]. A large value of n (~2) is an indication of cyclic DRX where as a low value of n (~1) conforms to single peak DRX. Therefore, based on the value of n, it could be suggested that alloy D9 exhibits single peak DRX. Sivaprasad et al. [14] have also reported single peak stress strain curve of this alloy during hot compression. The single peak DRX is also termed as growth controlled DRX [15] where a large number of

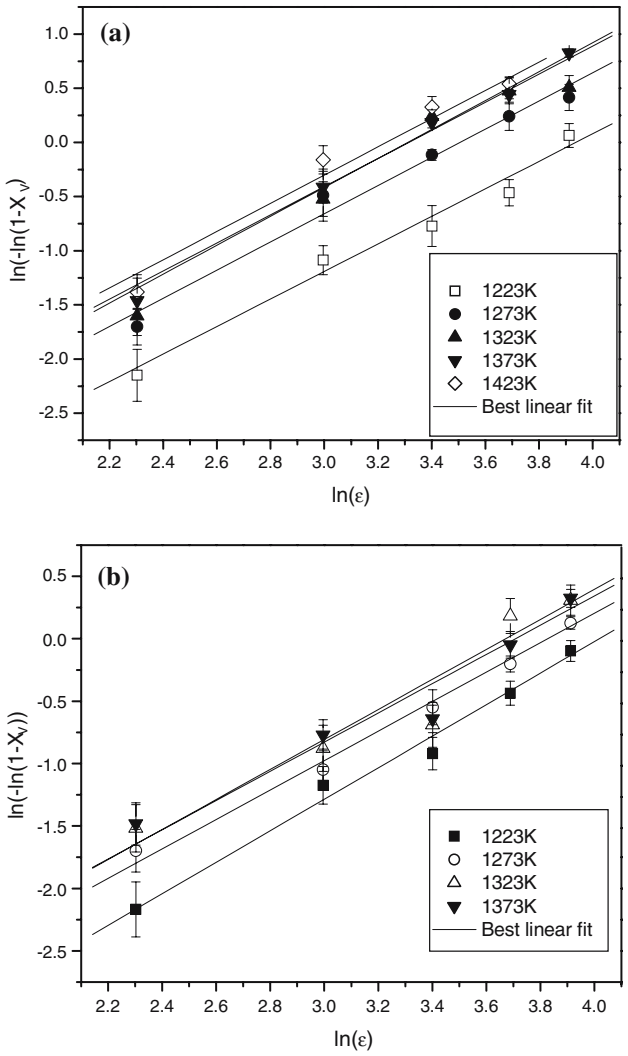

Fig. 2 Modified JMAK plot of recrystallization kinetics at various temperatures in (**a**) forge hammer and (**b**) hydraulic press operation

growing nuclei are formed and these growing nuclei mutually inhibit grain boundary. As a result grain growth is restricted that eventually leads to grain refinement. In the present study, the grain refinement mechanism is clearly manifested in microstructural investigation (Fig. 3) as well as grain size evaluation

Table 2 Avrami exponent (n) value at different hot working conditions in forge hammer and hydraulic press operation

Hot working temperature (K)	Avrami exponent value (n)	
	Forge hammer	Hydraulic press
1223	1.27	1.26
1273	1.30	1.18
1323	1.30	1.20
1373	1.34	1.17
1423	1.30	–

(Fig. 4a, b) which shows that after hot working, the resulting microstructure is always consisted of finer grain size as compare to starting one (starting average grain size was 200 μm).

Mechanism of DRX

At temperature of 1,223 K and at low strain levels, the microstructure consists of big grains (200 μm) and lamella like straight annealing twins (Fig. 3a). The dynamically recrystallized grains are hardly found in the matrix. At the same temperature and at moderate strain level, the grain boundaries become serrated in nature (Fig. 3b) which signifies the initiation of DRX in the deformed matrix. The curvy twin surface also indicates the initiation of DRX. The bulging of parent grain boundary and subsequent evolution of new DRX grain is clearly manifested in Fig. 3c. This signifies that nucleation of DRX takes place in the parent grain boundary by bulging mechanism. With increasing temperature, many DRX grains appear in the deformed matrix and incomplete necklace structures develop (Fig. 3d, e). At a temperature of 1,373 K and 0.3 strain level, as shown by Fig. 3f, more than half of the deformed matrix has been consumed by new DRX grains. Finally, at maximum temperature and strain level, the deformed grain structures have completely been disappeared and microstructure consisted of small equiaxed grains with average grain size of 45 μm (Fig. 3g). It could be noticed here that the fraction of DRX in the deformed matrix, manifested by optical micrograph, is showing similar kind of trend as found in Fig. 1 calculated based on hardness measurements method. So, it could be suggested that the hardness measurement method can be successfully applied to calculate the recrystallization fraction.

The bulging mechanism is able to describe how the first recrystallized grains and, correspondingly, the first layer of new recrystallized grains around the prior grains form. However, this mechanism could not be accounted for the expansion of the necklace structure through out the deformed matrix. This is because, in course of DRX when pre-existing grain boundaries are entirely covered by new grains (site saturation), bulging would have to proceed from the small recrystallized grains that requires a very high boundary curvature. This makes further nucleation by bulging unlikely, because the very high driving force necessary to offset the high surface tension of the bulge is not available in hot deformed microstructure [16].

The most crucial step for nucleation of DRX in the deformed matrix is generation of mobile grain boundary. The mobility increases with increasing misorientations,

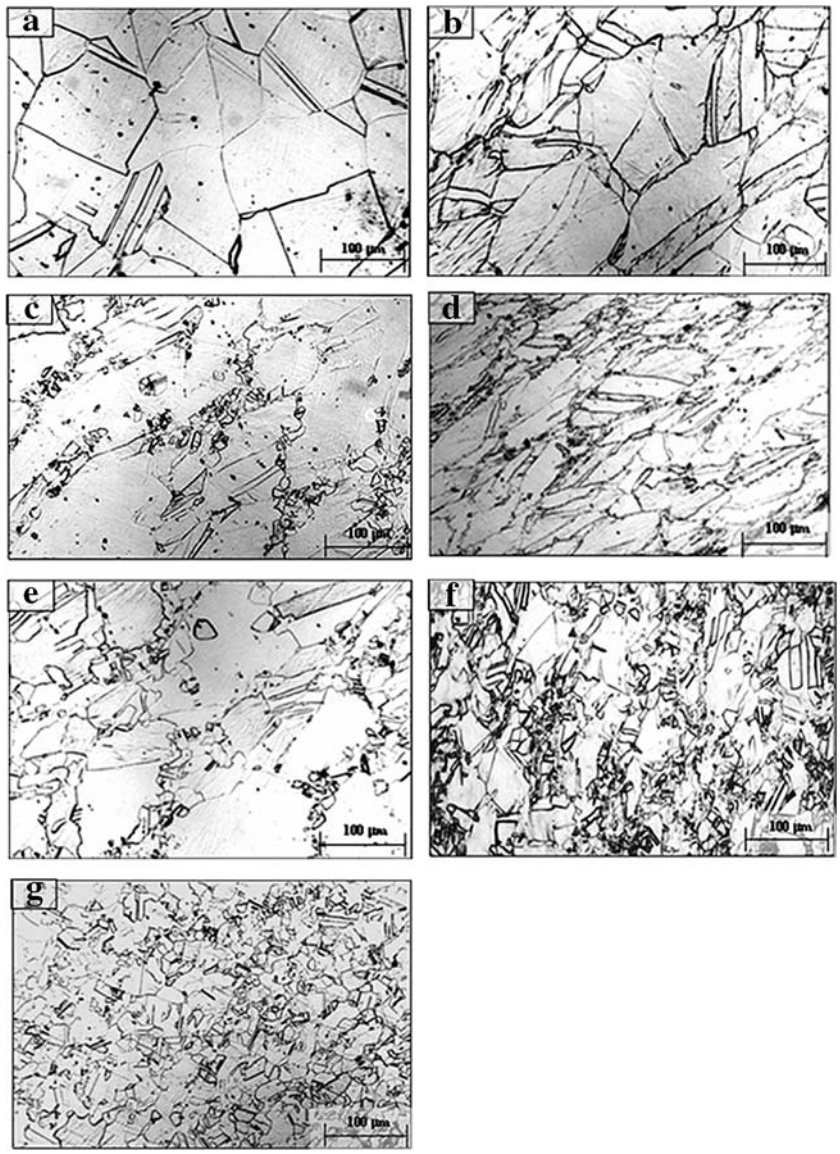

Fig. 3 Optical micrograph of alloy D9 (**a**) forge hammer: T = 1,223 K, ε = 0.07; (**b**) hydraulic press: T = 1,223 K, ε = 0.21; (**c**) forge hammer: T = 1,223 K, ε = 0.28; (**d**) hydraulic press: T = 1,273 K, ε = 0.27; (**e**) forge hammer: T = 1,273 K, ε = 0.28; (**f**) rolling: T = 1,373 K, ε = 0.3; and (**g**) forge hammer: T = 1,423 K, ε = 0.46

but a 10–15° misorientation is commonly assumed to be necessary. From the orientation image microscopy (OIM) map (Fig. 5) and corresponding misorientation distribution plot (Fig. 6), it has been seen that relative frequency of misorientations in excess of 10° were significantly low. On the other hand an appreciable amount of large misorientations (>55°) are observed in the matrix which could be accounted for twin boundaries [17, 18]. The substantial amounts of twins are also observed in optical micrograph. From the electron back scattered diffraction studies (EBSD), it has been observed that no significant texture component has been developed in the recrystallized volume. As can be seen from Fig. 7, the major texture component is only 4× random for {100}. This moderation of texture could be attributed to the repeated twining in the deformed matrix. Twining results in the formation of new grains with 60°, 180° or 300° rotated orientation around ⟨111⟩ axis with the parent grains. As all the directions except the direction of rotation axis are changed by the rotation operation, this means that no significant texture sharpening is expected unless the stable orientation of deformation is {111} [19]. However, the main component of texture developed in fcc metals is not {111}, but {011} [20, 21]. Furthermore, twin boundaries will constrain the orientations of the grain so that the texture will be reduced. Gottstein [22] has also reported that multiple twining results in moderation of texture in the matrix. So, from the present observations, it seems twin may play an important role during the nucleation and subsequent expansion of DRX in alloy D9, which in turn moderate the texture in the recrystallized matrix. The twining has also been identified as an active nucleation mechanism of DRX in alloy 800H (austenitic stainless steel) to promote

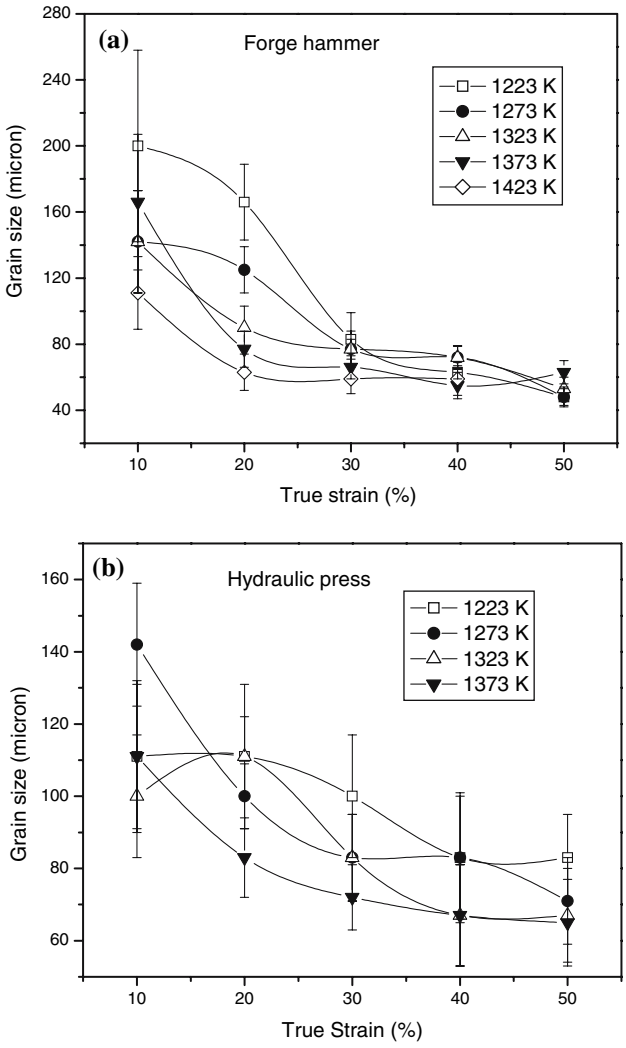

Fig. 4 Variation of average grain size with true strains at different temperatures in (**a**) forge hammer and (**b**) hydraulic press operation

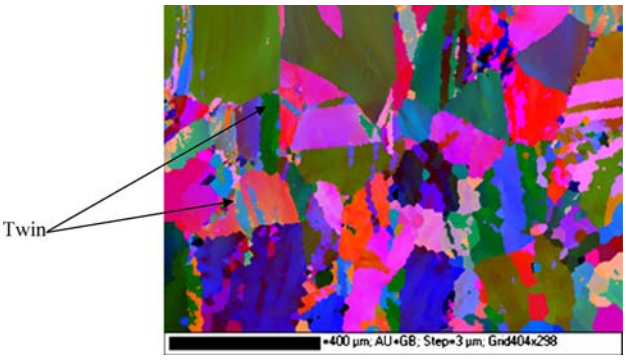

Fig. 5 Orientation image microscopy (OIM) map of the forge hammered sample hot worked at 1,273 K temperature with 0.2 strain

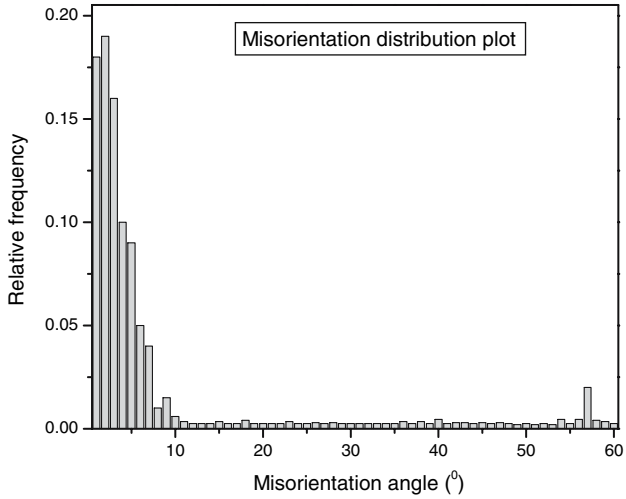

Fig. 6 Misorientation distribution plot of forge hammered sample hot worked at 1,273 K temperature with 0.2 strain

the expansion of the recrystallization front in course of DRX [23].

Grain size

As can be seen from the micrographs (Fig. 3), grain size evolution during DRX is complex in nature. When the extent of DRX is negligible (Fig. 3a), micrograph shows a single peak distribution of parent grains. However, at a higher extent of DRX, a clear bimodal distribution of grains can be observed (Fig. 3b–f). Some of these grains are equiaxed in nature while the others are elongated parent grains. Finally, again a single peak distribution of new equiaxed dynamically recrystallized grains are observed when the DRX process is almost completed (Fig. 3g). It is, therefore, clear that grain size distributions and aspect ratios are required in order to truly represent the DRX grains. However, this necessitates to include more input neurons in the neural network which would result in increased number of connection weights in the model. This would require more experimental data than that was considered in the present study. Therefore, we have considered the average grain size (along with the fraction of DRX) for the model with out losing relevant information about the developed microstructure.

Microstructural variables

From the DRX kinetics depicted in Fig. 1 as well as microstructural pattern illustrated in Fig. 3, it is evident that fraction of DRX increases with increase of temperature and strain. At the same time, strain rate

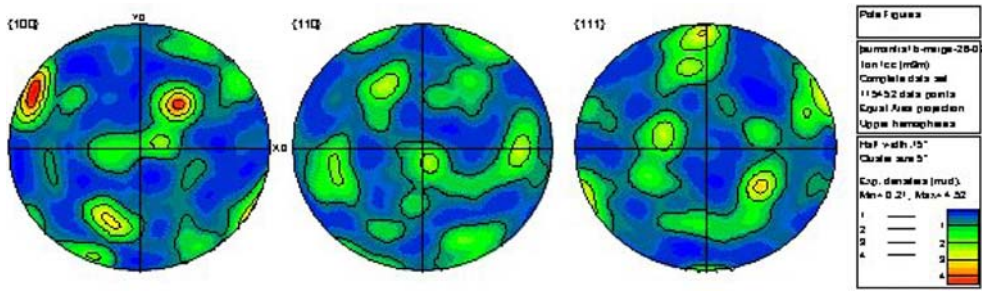

Fig. 7 Pole figure of forge hammered sample hot worked at 1,273 K temperature with 0.2 strain

is also playing a significant role to generate DRX volume in the product microstructure. The variation of average grain size with temperature, strain and strain rate is demonstrated in Fig. 4a, b. It could be seen that average grain size decreases with increase of strain and temperature.

So it could be suggested that a significant correlation between the process parameters and product microstructure exists. However, this interrelation is ambiguous and fuzzy in nature. Therefore, instead of conventional mathematical model, an ANN based model is employed to model the microstructural evolution of D9 alloy during hot forming. The input parameters of this model are strain, strain rate and temperature while microstructural features like fraction of DRX and grain size are obtained as output.

ANN model for microstructural evolution

In this study, a multilayer perceptron (MLP) based feed-forward ANN has been used since multilayer network has greater representational power for dealing with highly non-linear, strongly coupled, multivariable system [24]. One hidden layer is found adequate for present study. A logistic sigmoid function, presented by Eq. 6, is employed as the activation function; the learning is based on gradient descent algorithm and hence requires the activation function to be differentiable:

$$f(x) = \frac{1}{1 + \exp(-x)} \tag{6}$$

The MLP based feed-forward ANN is generally trained with back-propagation (BP) algorithm. In BP algorithm, the error between target output and the network output is calculated and this will be back propagated using the steepest descent or gradient descent approach. The network weights are adjusted by moving a small step in the direction of negative gradient of error surface during each iteration. The iterations are repeated until a specified convergence is reached. The convergence criterion for the network is determined by the average root-mean-square (RMS) error between the desired and predicted output values:

$$E_{\mathrm{RMS}} = \frac{1}{N}\sum_{i=1}^{N}\sqrt{\frac{1}{p}\sum_{j=1}^{p}(d_{ji} - y_{ji})} \tag{7}$$

where E_{RMS} is the average root-mean-square, N the number of training or testing data, p the number of variables in the output, and $d_j(n)$ and $y_j(n)$ are the target output and network output for neuron j respectively.

Though BP algorithm is being widely used, it has some inherent demerits. The BP algorithm uses an instantaneous estimate for the gradient of error surface in weight space. The algorithm is therefore stochastic in nature; that is, it has a tendency to zigzag its way about the true direction to a minimum on the error surface. Indeed, BP learning is an application of a statistical method known as stochastic approximation. Consequently, it tends to converge slowly and hence the back propagation networks with updated algorithms are used in the present study. The algorithms used are Resilient propagation (Rprop) and superSAB. A little description of the working of resilient propagation and superSAB algorithms is given below.

Rprop

Rprop is an effective learning algorithm that is based on direct adaptation of the weight step based on local gradient information. It does not consider, different from standard BP, the harmful influence of the absolute value of the partial derivative for the calculation of weight changes, but only the sign of the derivative to indicate the direction of weight update. If the derivative is positive (increasing error), the weight is decreased by its update value. On the other hand, if the derivative is negative, the update value is added. The algorithm can be mathematically expressed as follow [25]:

$$\Delta w_{ji}(n) = \begin{cases} -\Delta_{ji}(n), & \text{if } \dfrac{\partial E(n)}{\partial w_{ji}} > 0 \\ +\Delta_{ji}(n), & \text{if } \dfrac{\partial E(n)}{\partial w_{ji}} < 0 \\ 0, & \text{else} \end{cases} \tag{8}$$

$$w_{ji}(n+1) = w_{ji}(n) + \Delta w_{ji}(n)$$

$$\Delta_{ji}(n) = \begin{cases} \eta^{+}\Delta_{ji}(n-1), & \text{if } \dfrac{\partial E(n-1)}{\partial w_{ji}}\dfrac{\partial E(n)}{\partial w_{ji}} > 0 \\ \eta^{-}\Delta_{ji}(n-1), & \text{if } \dfrac{\partial E(n-1)}{\partial w_{ji}}\dfrac{\partial E(n)}{\partial w_{ji}} < 0 \\ \Delta_{ji}(n-1), & \text{else} \end{cases} \tag{9}$$

where $E(n)$ is the instantaneous value of total error energy; E_{av} is the average error energy; w_{ji} is the connection weight value, n denotes the number of iterations and $0 < \eta^{-} < 1 < \eta^{+}$.

As can be seen from the Eq. 8, the size of weight change is solely determined by the weight specific update value $\Delta_{ji}(n)$. Each time the partial derivative of the corresponding weight w_{ji} changes it sign, the $\Delta_{ji}(n)$ is decreased by a factor η^{-} (Eq. 9), since it is indicated that the last update was too large and the algorithm jumped over a local minimum. On the other hand, if the derivative retains its sign, the update value is slightly increased by the factor η^{+} in order to accelerate the convergence in shallow regions.

SuperSAB

The super self-adjusting back-propagation (superSAB) algorithm is based on the idea of sign-dependant learning rate adaptation. The basic of the function is to change the learning rate exponentially instead of linearly. This is done in order to take the wide range of temporarily suited learning rates into account [26].

In case of a change in sign of two successive derivatives, the previous weight is reversed. SuperSAB algorithm is considered to be fast convergence algorithm. It has been shown that superSAB converges orders of magnitude faster than the original back propagation algorithm, and is only slightly instable [27].

Predictability of model

The salient features of the model for fraction of DRX prediction is depicted in Table 3. The optimum structure is constructed by varying the number of hidden neurons from 1 to 20 and subsequently the network with minimum RMS error is said to be adequate for the present problem. It can be seen from the Table 3 that best outcome is obtained when the network is trained with Rprop learning algorithm. The corresponding correlation coefficient (R) for test dataset is found to be 0.984 (Fig. 8) which reflect that network can predict the fraction of DRX with good accuracy and reliability.

Table 3 The salient features of the model for fraction of DRX prediction in alloy D9

Learning algorithm	Number of hidden neurons	RMS test error (%)	Correlation coefficient (R)	Number of iterations
Rprop	12	4.31	0.984	400
SuperSAB	9	4.82	0.975	2400

The details of the model for grain size prediction have been summarized in Table 4. The results show that better performance is obtained when superSAB learning algorithm is employed. The predictability of the network is shown in the form of linear regression between the experimental data and corresponding predicted result for the test dataset (Fig. 9). It can be seen that experimental data tracks well with the predicted one. The deviation in correlation is about 5% and is shown by error bar. It can be observed that the prediction is quite accurate for the lower grain size range which corresponds to complete recrystallization (single peak distribution). A slight underestimation can be observed for the higher grain size which also corresponds to single peak distribution of parent grains. However, for the grain sizes in the range

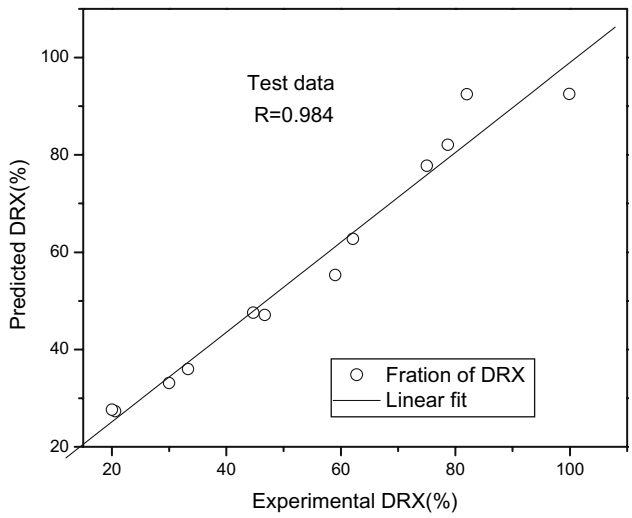

Fig. 8 Correlation between experimental and predicted test data for %DRX prediction employing Rprop learning algorithm

Table 4 The salient features of the model for grain size prediction in alloy D9

Learning algorithm	Number of hidden neurons	RMS test error (%)	Correlation coefficient (R)	Number of iterations
Rprop	8	7.31	0.945	500
SuperSAB	10	7.36	0.952	2700

80–100 μm, the deviation in prediction is significant. This may be due to the bimodal distribution of grains in this range as discussed earlier. However, this magnitude of the error in prediction, in fact, is less than the error that normally arises during grain size measurement as shown by error bar (one sigma confidence limit) in Fig. 4a, b. So the developed model can be applied for grain size prediction with reasonable accuracy.

From the above discussions, it could be suggested that both Rprop and superSAB algorithm can efficiently predict the microstructural features with reasonable accuracy and reliability. However, it has been found that Rprop required less number of iterations (Tables 3 and 4) and therefore is a faster convergence (~6 times faster) algorithm compare to superSAB.

Sensitivity analysis

It is often said that ANN is a ''black box'' because they are believed to provide very little explanatory insight into the relative contributions of input variables in the prediction processes. Recently a lot of work is being carried out to illuminate this black box [28, 29]. In this present study also, relative importance of the input variables is determined employing Garson's algorithm

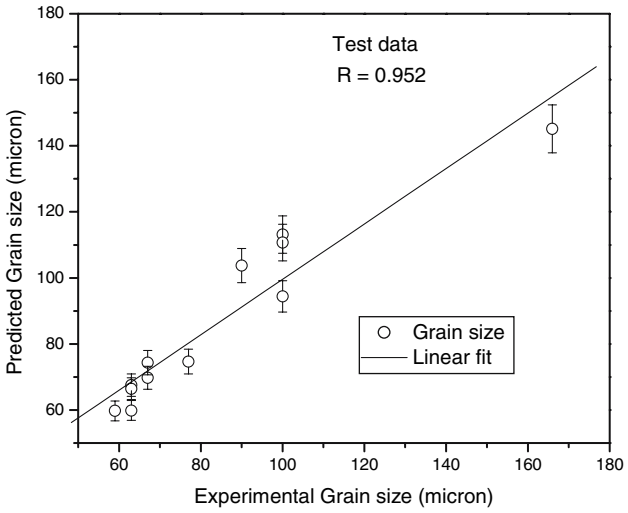

Fig. 9 Correlation between experimental and predicted test data for grain size prediction employing superSAB learning algorithm

Table 5 Relative importance (%) of input parameters based on Garson's algorithm

Predicted parameter	Temperature (%)	Strain (%)	Strain rate (%)
%DRX	26.70	47.26	26.04
Grain size	19.65	38.26	42.09

[30]. The method essentially involves partitioning the hidden-output connection weights into components associated with each input neuron using absolute values of connection weights. The relative importance of individual parameters for fraction of DRX and grain size prediction is depicted in Table 5. The results show that strain is the most significant parameter for dynamic recrystallization while both strain and strain rate contribute substantially for grain size. In fact, the effect of strain on fraction of DRX and grain size is well manifested in Figs. 1 and 4.

Conclusions

Based on the present investigation, the following conclusions can be drawn:

- The kinetics of DRX in alloy D9 have been studied using modified JMAK model represented by the equation: $X_v = 1 - \exp(-k\varepsilon^n)$. The experimental recrystallization kinetics measurements of alloy D9 have been found to agree with the modified JMAK model.
- The value of Avrami exponent closely varies between 1.17 and 1.34 which signifies that alloy D9 exhibits growth controlled DRX.
- The microstructural study shows that nucleation of new grains during DRX takes place on the parent grain boundary by bulging mechanism.
- No significant texture component has been developed in the recrystallized matrix as revealed by EBSD. This may be attributed to twin boundaries that constrain the orientation of the grains and thereby reduce the texture. A substantial amount of twin has also been identified in DRX matrix by optical micrograph and OIM. Therefore, it seems twins may play an important role during the nucleation and subsequent expansion of DRX in alloy D9, which in turn moderate the texture in the recrystallized matrix.
- A significant correlation between microstructural features and process parameters has been found. However, this interrelation is ambiguous and hence fuzzy in nature.

- A model for the microstructural evolution, including the fraction of DRX and grain size, has been established employing ANN. Instead of standard BP algorithm, the network has been trained with two upgraded algorithm viz. Rprop and superSAB. Both the algorithm can predict the microstructural features with reasonable accuracy and reliability. However, Rprop is found to be a faster convergence algorithm compare to superSAB.
- An instantaneous microstructure can be designed from the developed model in order to optimize the process parameters based on microstructural evolution.

Acknowledgements The authors would like to express their sincere thanks to Dr. S. Venugopal, Head, Metal Forming & Tribology Section and Dr. S.K. Ray, Head, Materials Technology Division for useful discussions. The authors also gratefully acknowledge Dr. S.L. Mannan, Director, Metallurgy & Materials Group and Dr. Baldev Raj, Director, Indira Gandhi Centre for Atomic Research (IGCAR) for their constant encouragement throughout the course of this work. The authors also thank the reviewers for making very useful suggestions/comments.

References

1. Mannan SL, Sivaprasad PV (2001) In: Jurgen Buschow KH, Cahn RW, Flemings MC, Ilschner B, Kramer EJ, Mahajan S (eds) Encyclopedia of materials science and technology, vol 3. Elsevier, New York, pp 2857–2865
2. Venkadesan S, Sivaprasad PV, Narayanan C, Shanmugam V (1992) In: Rao PK et al (eds) Proceedings of the international conference on stainless steels INCOSS-89, Ind Inst Metals, Bombay, Feb 1989. Omega Scientific Publishers, New Delhi, pp 345-360
3. Wang X, Brunger E, Gottstein G (2002) Scr Mater 46:875
4. Belyakov A, Miura H, Sakai T (2000) Scr Mater 43:21
5. Sivaprasad PV (1997) PhD Thesis, IIT Bombay
6. Miaoquan L, Aiming X, Weichao H (2003) Mater Character 49:203
7. Sakai T, Ohashi M, Chaiba K (1988) Acta Metal 36(7):1781
8. Liu WC, Morris JG (2005) Mater Sci Eng A 402:215
9. Weiping Y, Gall RL, Saindrenan G (2002) Mater Sci Eng A 332:41
10. Prasad YVRK, Ravichandran N (1991) Bull Mater Sci 14:1241
11. Mandal S, Sivaprasad PV, Venugopal S, Murthy KPN (2006) Modelling Simul Mater Sci Eng 14:1053
12. Venugopal S, Sivaprasad PV, Venkadesan S, Effect of annealing temperature on engineering properties of alloy D9, unpublished work
13. Wahabi M, Cabrera JM, Prado JM (2003) Mater Sci Eng A 343:116
14. Sivaprasad PV, Mannan SL, Prasad YVRK, Chaturvedi RC (2002) Mater Sci Technol 17:545
15. Sakai T, Jonas JJ (1984) Acta Metal 32(2):189
16. Ponge D, Gottstein G (1998) Acta Mater 46(1):69
17. Karduck P, Gottstein G, Mecking H (1983) Acta Mater 31:1525
18. Brunger E, Wang X, Gottstein G (1998) Scr Mater 38(12):1843
19. Hasegawa M, Yamamoto M, Fukutomi H (2003) Acta Mater 51:3939
20. Barrett CS, Levenson LH (1940) Trans AIME 137:112
21. Hasegawa M, Fukutomi H (2002) Mater Trans 43:2243
22. Gottstein G (1984) Acta Metal 32:1117
23. Wang X, Brunger E, Gottstein G (2002) Scr Mater 46:875
24. Juang SC, Tarang YS, Lii HR (1998) J Mater Process Technol 75:54
25. Reidimiller M, Braun H (1993) Proceedings of the international conference in neural networks, San Francisco, CA
26. Reidimiller M (1994) Special issue on Neural Netw 5
27. Tollenaere T (1990) Neural Netw 3(5):561
28. Olden JD, Jackson DA (2002) Ecol Model 154:135
29. Gevrey M, Dimopoulos I, Lek S (2003) Ecol Model 160:249
30. Garson GD (1991) Artif Intell Expert 6:47